

# Cross Modal Transformer via Coordinates Encoding for 3D Object Detection

Junjie Yan    Yingfei Liu    Jianjian Sun    Fan Jia    Shuailin Li  
 Tiancai Wang    Xiangyu Zhang  
 MEGVII Technology

## Abstract

In this paper, we propose a robust 3D detector, named Cross Modal Transformer (CMT), for end-to-end 3D multi-modal detection. Without explicit view transformation, CMT takes the image and point clouds tokens as inputs and directly outputs accurate 3D bounding boxes. The spatial alignment of multi-modal tokens is performed implicitly, by encoding the 3D points into multi-modal features. The core design of CMT is quite simple while its performance is impressive. CMT obtains 73.0% NDS on nuScenes benchmark. Moreover, CMT has a strong robustness even if the LiDAR is missing. Code will be released at <https://github.com/junjie18/CMT>.

## 1. Introduction

Multi-sensor fusion has shown its great superiority in autonomous driving system [1, 8, 20, 24, 28]. Different sensors usually provide the complementary information for each other. For instance, the camera captures information in a perspective view and the image contains rich semantic features while point clouds provide much more localization and geometry information. Taking full advantage of different sensors helps reduce the uncertainty and makes accurate and robust prediction.

Sensor data of different modalities usually has large discrepancy in distribution, making it hard to merge the multi-modalities. State-of-the-art (SoTA) methods tend to fuse the multi-modality by constructing unified bird's-eye-view (BEV) representation [20, 24, 28] or querying from tokens [1, 8]. For example, BEVFusion [28] explores a unified representation by BEV transformation for BEV feature fusion (see Fig. 1(a)). TransFusion [1] follows a two-stage pipeline and the camera images in second stage provide supplementary information for prediction refinement (see Fig. 1(b)). However, exploring a truly end-to-end pipeline for multi-sensor fusion remains to be a question.

Recently, the effectiveness of end-to-end object detection with transformer (DETR) [3, 56] has been proved in many perception tasks, such as instance segmentation [10,

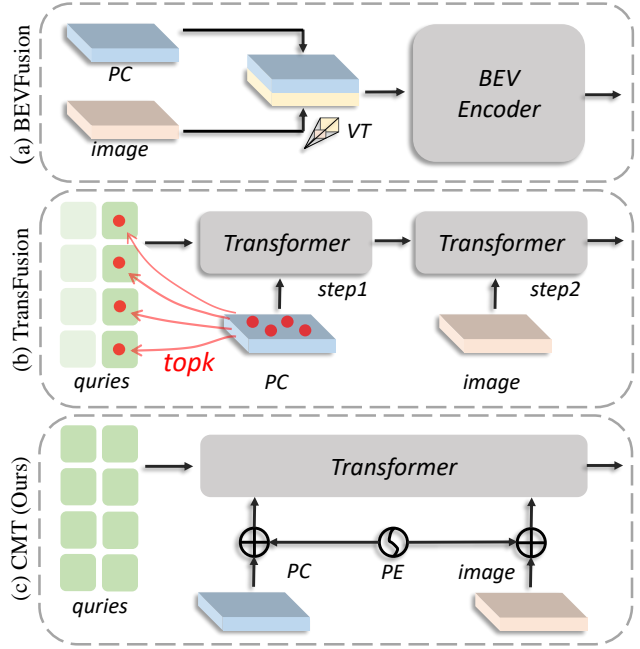


Figure 1. Comparison between BEVFusion, TransFusion, and our proposed CMT. (a) In BEVFusion, the camera features are transformed into BEV space by view transform. Two modality features are concatenated in BEV space and the BEV encoder is adopted for fusion. (b) TransFusion first generates the queries from the high response regions of LiDAR features. After that, object queries interact with point cloud features and image features separately. (c) In CMT, the object queries directly interact with multi modality features simultaneously. Position encoding (PE) is added to the multi-modal features for alignment. "VT" is the view transformation from image to 3D space.

12], multi-object tracking [30, 51] and visual 3D detection [26, 27, 45]. The DETR architecture is simple yet effective thanks to the object queries for representing different instances and bipartite matching for one-to-one assignment.

Inspired by DETR, we aim to build an elegant end-to-end pipeline for multi-modal fusion in 3D object detection. In DETR, object queries directly interact with the image tokens through cross-attention in transformer decoder. For 3D

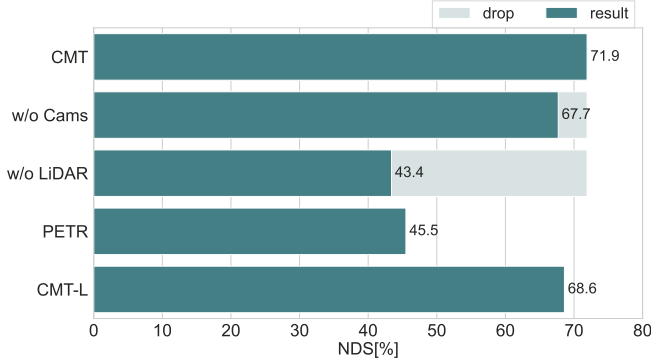


Figure 2. CMT has a strong robustness under sensor missing condition. During inference, CMT without LiDAR achieves similar detection performance compared to the SoTA camera-only detector PETR [26]. CMT without camera input only introduce a slight drop, compared to our LiDAR-only baseline CMT-L. (Note: we evaluate without any finetune process)

object detection, one intuitive way is to concatenate the image and point cloud tokens together for further interaction with object queries. However, the concatenated tokens are disordered and unaware of their corresponding locations in 3D space. Therefore, it is necessary to provide the location prior for multi-modal tokens and object queries.

In this paper, we propose Cross-Modal Transformer (CMT), a simple yet effective end-to-end pipeline for high-performance 3D object detection (see Fig. 1(c)). First, we propose the Coordinates Encoding Module (CEM), which produces position-aware features, by encoding 3D points set implicitly into multi-modal tokens. Specifically, for camera images, 3D points sampled from frustum space are used to indicate the probability of 3D positions for each pixel. While for LiDAR, the BEV coordinates are simply encoded into the point cloud tokens. Next, we introduce the position-guided queries. Each query is initialized as a 3D reference point following PETR [26]. We transform the 3D coordinates of reference points to both image and LiDAR spaces, to perform the relative coordinates encoding in each space. Moreover, for faster convergence, we introduce the inductive bias of locality, by extending Query Denoising [19] to a point-based formulation.

The proposed CMT framework brings many advantages compared to existing methods. Firstly, our method is a simple and end-to-end pipeline and can be easily extended. The 3D positions are encoded into the multi-modal features implicitly, which avoids introducing the bias caused by explicit cross-view feature alignment. Secondly, our method only contains basic operations, without the feature sampling or complex 2D-to-3D view transformation on multi-modal features. Thirdly, the robustness of our CMT is much stronger than other existing approaches. Extremely, under the condition of LiDAR miss, our CMT with only image

tokens can achieve similar performance compared to those visual 3D object detectors [23, 26] (see Fig. 2).

To summarize, our contributions are:

- we propose a robust 3D detector, which is a truly end-to-end framework without any post-process. It overcomes the sensor missing problem.
- The 3D positions are implicitly encoded into the multi-modal tokens, without any complex operations, like grid sampling and voxel-pooling.
- CMT achieves state-of-the-art 3D detection performance on nuScenes dataset. It provides a simple baseline for future research.

## 2. Related Work

### 2.1. Camera Based 3D Object Detection

Camera-based 3D object detection is one of the basic tasks in computer vision. Early works [41, 42] mainly follow the dense prediction pipeline. They first localize the objects on image plane and then predict their relevant 3D attributes, such as depth, size and orientation. However, with the surrounding cameras, the perspective-view based design requires elaborate post-processes to eliminate the redundant predictions of the overlapping regions. Recently, 3D object detection under the BEV has attracted increasing attention. The BEV representation provides a unified coordinate to fuse information from multiple camera views. LSS [32], BEVDet [15] and BEVDepth [21] predict the depth distribution to lift the image features to 3D frustum meshgrid. Besides, inspired by DETR [4], DETR3D [45] and BEVFormer [23] project the predefined BEV queries onto images and then employ the transformer attention to model the relation of multi-view features. The above methods explicitly project the local image feature from 2D perspective view to BEV. Different from them, PETR [26, 27] and SpatialDETR [9] adopt the positional embedding that depends on the camera poses, allowing the transformer to implicitly learn the projection from image views to 3D space.

### 2.2. LiDAR Based 3D Object Detection

LiDAR-based 3D object detection aims to predict 3D object bounding boxes using the point clouds captured from LiDAR. Existing methods process the point cloud into different representations. Point-based methods [22, 33–36, 49] directly extract features from raw point clouds and predict 3D bounding boxes. PointNet [34] is the first architecture to process the point cloud in an end-to-end manner, which preserves the spatial characteristics of the point cloud. Other methods project the unordered, irregular LiDAR point clouds onto a regular feature space such as 3D voxels [54], feature pillars [17, 44, 50] and range images [11, 38]. Then the features are extracted in the BEV

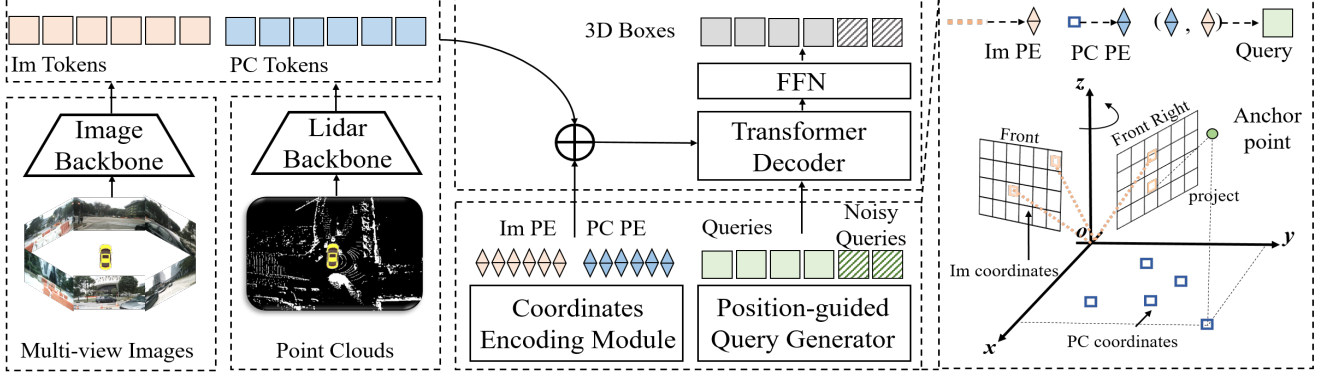


Figure 3. The architecture of Cross-Modal Transformer (CMT) paradigm. The multi-view images and point clouds are input to two backbone networks to extract feature tokens. In coordinates encoding module, coordinates of camera rays and BEV positions are transformed into the image position encoding (Im PE) and point cloud position encoding (PC PE), respectively. The queries are generated by the position-guided query generator. In query generator, 3D anchor points are projected to different modalities and the relative coordinates are encoded (see the right part). Multi-modal tokens further interact with queries in the transformer decoder. The updated queries are further used to predict the 3D bounding boxes. To accelerate the model convergence, the point-based query denoising is introduced.

plane using a standard 2D backbone. VoxelNet [54] first divides the raw point clouds into regular voxel grids, and then uses PointNet network to extract features from the points in each voxel grid.

### 2.3. Multi-modal 3D Object Detection

Multi-sensor fusion in 3D detection has gained great attention in recent years. State-of-the-art (SoTA) methods tend to find a unified representation for both modalities, or define object queries to fuse the features for further prediction. For example, BEVFusion [24, 28] applies a lift-splat-shoot (LSS) operation to project image feature onto BEV space and concatenates it with LiDAR feature. UVTR [20] generates a unified representation in the 3D voxel space by deformable attention [56]. While for query-based methods, FUTR3D [8] defines the 3D reference points as queries and directly samples the features from the coordinates of projected planes. TransFusion [1] follows a two-stage pipeline. The proposals are generated by LiDAR features and further refined by querying the image features.

### 2.4. Transformer-based Object Detection

The pioneering work DETR [3] proposes a transformer-based detector paradigm without any hand-craft components, and has achieved state-of-the-arts in both 2D and 3D detection [6, 23, 27, 53]. However, DETR-like methods usually suffer from the slow convergence. To this end, many works [5, 16, 19, 25, 52, 53, 56] are proposed to improve the training efficiency from various aspects. Other improvements in 2D detection mainly focus on modifying the transformer layers [52, 56], designing informative object queries [19, 25, 53], or exploring the label assignment mechanism [5, 16]. Deformable DETR [56] proposes the de-

formable attention, which only attends to sampling points of local regions. SAM-DETR [52] presents a semantic aligner between object queries and encoded features to accelerate the matching process. To alleviate the instability of bipartite matching, DAB-DETR [25] formulates the object queries as dynamic anchor boxes, while DN-DETR [19] auxillarily reconstructs the ground-truths from the noisy ones. Based on them, DINO [53] further improves the denoising anchor boxes via a contrastive way.

## 3. Method

The overall architecture of the proposed CMT is illustrated in Fig. 3. Multi-view images and LiDAR points are fed into two individual backbones to extract multi-modal tokens. The 3D coordinates are encoded into the multi-modal tokens by the *coordinates encoding*. The queries from the *position-guided query generator* are used to interact with the multi-modal tokens in transformer decoder and then predict the object class as well as the 3D bounding boxes. *Point-based query denoising* is further introduced to accelerate the training convergence by introducing local prior. The whole framework is learned in a fully end-to-end manner and LiDAR backbone is trained from scratch without pretraining.

### 3.1. Coordinates Encoding Module

The coordinates encoding module (CEM) is used to encode the 3D position information into multi-modal tokens. It generates both the camera and BEV position encodings (PEs), which are added to image tokens and point cloud tokens respectively. With the help of CEM, multi-modal tokens can be implicitly aligned in 3D space.

Let  $P(u, v)$  be the 3D points set corresponding to the

feature map  $F(u, v)$  of different modalities. Here  $(u, v)$  indicates the coordinate in the feature map. Specifically,  $F$  is the image feature for camera while BEV feature for LiDAR. Suppose the output position embedding of CEM is  $\Gamma(u, v)$ , its calculation can be formulated as:

$$\Gamma(u, v) = \psi(P(u, v)) \quad (1)$$

where  $\psi$  is a multi-layer perception (MLP) layer.

**CE for Images.** Since the image is captured from a perspective view, each pixel can be seen as an epipolar line in 3D space. Inspired by PETR [26], for each image, we encode a set of points in camera frustum space to perform the coordinates encoding. Given the image feature  $F_{im}$ , each pixel can be formulated as a series of points  $\{p_k(u, v) = (u * d_k, v * d_k, d_k, 1)^T, k = 1, 2, \dots, d\}$  in the camera frustum coordinates. Here,  $d$  is the number of points sampled along the depth axis. The corresponding 3D points can be calculated by:

$$p_k^{im}(u, v) = T_{c_i}^l K_i^{-1} p_k(u, v) \quad (2)$$

where  $T_{c_i}^l \in R^{4 \times 4}$  is the transformation matrix from the  $i$ -th camera coordinate to the LiDAR coordinate.  $K_i \in 4 \times 4$  is the intrinsic matrix of  $i$ -th camera. The position encoding of pixel  $(u, v)$  for image is formulated as:

$$\Gamma_{im}(u, v) = \psi_{im}(\{p_k^{im}(u, v), k = 1, 2, \dots, d\}) \quad (3)$$

**CE for Point Clouds.** We choose VoxelNet [48, 54] or PointPillar [17] as backbone to encode the point cloud tokens  $F_{pc}$ . Intuitively, the point set  $P$  in Eq. (1) can be sampled along the Z-axis. Suppose  $(u, v)$  is the coordinates in BEV feature map, the sampled point set is then  $p_k(u, v) = (u, v, h_k, 1)^T$ , where  $h_k$  indicates the height of  $k$ -th points and  $h_0 = 0$  as default. The corresponding 3D points of BEV feature map can be calculated by:

$$p_k^{pc}(u, v) = (u * u_d, v * v_d, h_k, 1) \quad (4)$$

where  $(u_d, v_d)$  is the size of each BEV feature grid. To simplify, we only sample one point along the height axis. It is equivalent to the 2D coordinate encoding in BEV space. The position embedding of point cloud can be obtained by:

$$\Gamma_{pc}(u, v) = \psi_{pc}(\{p_k^{pc}(u, v), k = 1, 2, \dots, h\}) \quad (5)$$

### 3.2. Position-guided Query Generator

Following Anchor-DETR [46] and PETR [26], we firstly initialize the queries with  $n$  anchor points  $A = \{a_i = (a_{x,i}, a_{y,i}, a_{z,i}), i = 1, 2, \dots, n\}$  sampled from uniform distribution between  $[0, 1]$ . Then these anchor points are transformed into 3D world space by linear transformation:

$$\begin{cases} a_{x,i} = a_{x,i} * (x_{max} - x_{min}) + x_{min} \\ a_{y,i} = a_{y,i} * (y_{max} - y_{min}) + y_{min} \\ a_{z,i} = a_{z,i} * (z_{max} - z_{min}) + z_{min} \end{cases} \quad (6)$$

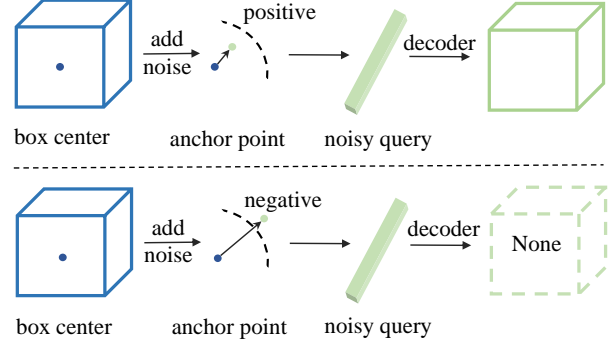


Figure 4. Illustration of the proposed point-based query denoising. The noise queries are generated from the box center of ground-truths. The positive and negative queries are split by the noise scale. Positive queries are used to reconstruct the ground-truths boxes, while negative queries predict the “no object”.

where  $[x_{min}, y_{min}, z_{min}, x_{max}, y_{max}, z_{max}]$  is the region of interest (RoI) of 3D world space. After that, we project the 3D anchor points  $A$  to different modalities and encode the corresponding point sets by CEM. Then the positional embedding  $\Gamma_q$  of object queries can be generated by:

$$\Gamma_q = \psi_{pc}(A_{pc}) + \psi_{im}(A_{im}) \quad (7)$$

where  $A_{pc}$  and  $A_{im}$  are the point set projected on BEV plane and image plane, respectively. The positional embedding  $\Gamma_q$  are further added with the query content embedding to generate the initial position-guided queries  $Q_0$ .

### 3.3. Point-based Query Denoising (PQD)

For fast convergence, we extend the query denoising strategy in DN-DETR [19] to 3D object detection as shown in Fig. 4. Different from DN-DETR [19], we generate the noisy anchor points by center shifting since the box scale is not that important in 3D object detection. For each 3D ground-truths box  $(x, y, z, w, l, h, \theta)$ , we first sample the random ratio  $\lambda_1, \lambda_2, \lambda_3$  within  $(-\lambda, \lambda)$ , where  $\lambda$  is the hyper-parameter to control the noise scale. Since 3D space is sparse and unobstructed, we adopt a larger tolerance (e.g.  $\lambda = 1.0$ ). Then the center noise  $(\Delta x, \Delta y, \Delta z)$  can be calculated as:

$$\Delta x = \frac{\lambda_1 w}{2}, \Delta y = \frac{\lambda_2 l}{2}, \Delta z = \frac{\lambda_3 h}{2}. \quad (8)$$

The center noise is added to the center of ground-truths to obtain the noise anchor points. Then each noise anchor point can be converted into noise query, as described in the last section. Inspired by DINO [53], we also introduce the negative noisy queries to predict the “no object”. To simplify the pipeline, the positive and negative queries are simply split by the random ratios  $\lambda_1, \lambda_2, \lambda_3$  and a given threshold  $\xi$ . For each noise query, it is a positive query if  $\sqrt{\lambda_1^2 + \lambda_2^2 + \lambda_3^2} < \xi$ , otherwise a negative query.

Table 1. Performance comparison on the nuScenes **test** set. “L” is LiDAR and “C” is camera.

Methods	Modality	NDS↑	mAP↑	mATE↓	mASE↓	mAOE↓	mAVE↓	mAAE↓
BEVDet [15]	C	0.488	0.424	0.524	0.242	0.373	0.950	0.148
DETR3D [45]	C	0.479	0.412	0.641	0.255	0.394	0.845	0.133
PETR [26]	C	0.504	0.441	0.593	0.249	0.383	0.808	0.132
CenterPoint [50]	L	0.673	0.603	0.262	0.239	0.361	0.288	0.136
UVTR [20]	L	0.697	0.639	0.302	0.246	0.350	0.207	0.123
TransFusion [1]	L	0.702	0.655	0.256	0.240	0.351	0.278	0.129
PointPainting [39]	LC	0.610	0.541	0.380	0.260	0.541	0.293	0.131
PointAugmenting [40]	LC	0.711	0.668	0.253	0.235	0.354	0.266	0.123
MVP [7]	LC	0.705	0.664	0.263	0.238	0.321	0.313	0.134
FusionPainting [47]	LC	0.716	0.681	0.256	0.236	0.346	0.274	0.132
UVTR [20]	LC	0.711	0.671	0.306	0.245	0.351	0.225	0.124
TransFusion [1]	LC	0.717	0.689	0.259	0.243	0.359	0.288	0.127
BEVFusion [28]	LC	0.729	0.702	0.261	0.239	0.329	0.260	0.134
CMT-L	L	<b>0.701</b>	<b>0.646</b>	0.298	0.242	0.330	0.222	0.124
CMT	LC	<b>0.730</b>	<b>0.704</b>	0.299	0.241	0.323	0.240	0.112

Table 2. Performance comparison on the nuScenes **val** set. “L” is LiDAR and “C” is camera.

Methods	modality	NDS↑	mAP↑
FUTR3D [8]	L	0.655	0.593
UVTR [20]	L	0.676	0.608
TransFusion [1]	L	0.702	0.655
FUTR3D [8]	LC	0.683	0.645
UVTR [20]	LC	0.702	0.654
TransFusion [1]	LC	0.713	0.675
BEVFusion [28]	LC	0.714	0.685
CMT-L	L	0.686	0.624
CMT	LC	<b>0.719</b>	<b>0.694</b>

### 3.4. Decoder and Loss

As for the decoder, we follow the original transformer decoder in DETR [46] and use  $L$  decoder layers. For each decoder layer, the position-guided queries interact with the multi-modal tokens and update their representations. Two feed-forward networks (FFNs) are used to predict the 3D bounding boxes and the classes using updated queries. We formulate the prediction process of each decoder layer as follows:

$$\hat{b}_i = \Psi^{reg}(Q_i), \hat{c}_i = \Psi^{cls}(Q_i), \quad (9)$$

where  $\Psi^{reg}$  and  $\Psi^{cls}$  respectively represent the FFN for regression and classification.  $Q_i$  is the the updated object queries of the  $i$ -th decoder layer.

For set prediction, the bipartite matching is applied for one-to-one assignment between predictions and ground-

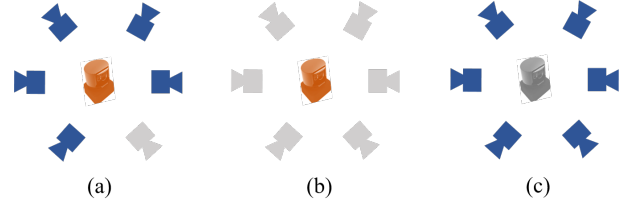


Figure 5. We analyze the system robustness of CMT at test period under three simulated sensor errors: (a) single camera miss, (b) all camera miss and (c) LiDAR miss.

truths. We adopt the focal loss for classification and  $L1$  loss for 3D bounding box regression:

$$L(y, \hat{y}) = \omega_1 L_{cls}(c, \hat{c}) + \omega_2 L_{reg}(b, \hat{b}) \quad (10)$$

where  $\omega_1$  and  $\omega_2$  are the hyper-parameter to balance the two loss terms. Note that for positive and negative queries in query denoising, the loss is calculated in the same way.

### 3.5. Masked-Modal Training for Robustness

Security is the most important concern for autonomous driving systems. An ideal system requires solid performance even if part of them fails, as well as not relying on any input of a specific modality. Recently, BEVFusion [24] has explored the robustness of LiDAR sensor failure. However, the exploration is limited to restricted scan range and model need be retrained. In this paper, we try more extreme failures, including single camera miss, camera miss and LiDAR miss, as shown in Fig. 5. It is consistent with the actual scene and ensures the safety of autonomous driving.



Table 3. Quantitative results on the nuScenes val with LiDAR or camera miss. With the masked-modal training, the efficacy and robustness of our CMT is significantly improved, especially when the LiDAR camera is missed.

Metric	Vanilla training			Masked-modal training		
	CMT	only LiDAR	only Cams	CMT	only LiDAR	only Cams
NDS $\uparrow$	0.716	0.594	0.067	0.719 ( $\uparrow 0.3\%$ )	0.677 ( $\uparrow 8.3\%$ )	0.434 ( $\uparrow 36.7\%$ )
mAP $\uparrow$	0.685	0.472	0.000	0.694 ( $\uparrow 0.9\%$ )	0.613 ( $\uparrow 14.1\%$ )	0.386 ( $\uparrow 38.6\%$ )

To improve the robustness of the model, we propose a training strategy, called masked-modal training. In training process, we randomly use only a single modality for training, such as camera or LiDAR, with the ratio of  $\eta_1$  and  $\eta_2$ . This strategy ensures that the model are fully trained with both single modal and multi-modal. Then the model can be tested with single modal or multi-modal, without modifying the model weight. The experimental results show that masked-modal training will not affect the performance of our fusion model. Even if LiDAR is damaged, it can still achieve similar performance compared to SoTA range-view 3D detectors [15, 26].

## 4. Experiments

### 4.1. Datasets and Metrics

We evaluate our method on nuScenes [2]. nuScenes is a large-scale multi-modal dataset, which is composed of data from 6 cameras, 1 LiDAR and 5 radars. The dataset has 1000 scenes totally and is divided into 700/150/150 scenes as train/validation/test sets, respectively.

**Cameras.** Each scene has 20s video frames with 12 FPS. 3D bounding boxes are annotated every 0.5s. We only use these key frames. In each frame, nuScenes provides images from six cameras.

**LiDAR.** NuScenes provides a 32-beam LiDAR with 20 FPS. The key frames are also annotated every 0.5s, the same as cameras. We follow the common practice to transform the points from the past 9 frames to the current frame for training and evaluation.

**Metrics.** We follow the nuScenes official metrics. We report the nuScenes Detection Score (NDS), mean Average Precision (mAP), mean Average Translation Error (mATE), mean Average Scale Error (mASE), mean Average Orientation Error (mAOE), mean Average Velocity Error (mAVE) and mean Average Attribute Error (mAAE).

### 4.2. Implementation Details

We use ResNet [13] or VoVNet [18] as image backbone to extract the 2D image features. The C5 feature is up-sampled and fused with C4 feature to produce P4 feature. We use VoxelNet [54] or PointPillars [17] as the backbone to extract the point-cloud features. We set the region-of-interest (RoI) to  $[-54.0m, 54.0m]$  for X and Y axis, and

$[-5.0m, 3.0m]$  for Z axis. The 3D coordinates in the world space are normalized to  $[0, 1]$ . All the feature dimension is set to 256, including the LiDAR feature, image feature and query embedding. Six decoder layers are adopted in transformer decoder. Voxel size of 0.075 and image size of  $1600 \times 640$  are adopted as default in our experiments.

Our model is trained with the batch size of 16 on 8 A100 GPUs. It is trained for total 20 epochs with CBGS [55]. We adopt the AdamW [29] optimizer for optimization. The initial learning rate is  $1.0 \times 10^{-4}$  and we follow the cycle learning rate policy [37]. The mask ratios  $\eta_1$  and  $\eta_2$  are both set to 0.25 for masked-modal training. The threshold  $\xi$  is set to 0.75 to divide the noise queries into positives and negatives for training. The tolerance  $\lambda$  that controls the noise scale is set to 1. The GT sample augmentation is employed for the first 15 epochs and closed for the rest epochs. As for the loss weights, we follow the default setting in DETR3D [45] and set the  $\omega_1$  and  $\omega_2$  to 2.0 and 0.25, respectively.

### 4.3. State-of-the-Art Comparison

As shown in Tab. 1, CMT achieves comparable results compared to several state-of-the-art methods on nuScenes test set. Our LiDAR-only baseline, named CMT-L, achieves the 70.1% NDS, which is a nearly SoTA performance among all existing LiDAR-only methods. Our multi-modal method CMT achieves 73.0% NDS and 70.4% mAP and outperforms existing SoTA BEVFusion. Benefits from the large receptive field, CMT gains better results on some metrics like mAVE. We also compare the performance with other SoTA methods on nuScenes val set (see Tab. 2). It shows that our proposed CMT with multi-modal fusion outperforms the BEVFusion by 0.5% NDS and 0.9% mAP. CMT introduces large performance improvements compared to our LiDAR-only CMT-L by 2.9%/5.8% and 3.3%/7.0% NDS/mAP on test and validation set, showing that camera images bring complementary information.

### 4.4. Strong Robustness

We evaluate the robustness of our framework under various harsh environments, including LiDAR miss and camera miss. Tab. 3 shows the results when the sensor miss occurs, by simulating the scenarios of any modality totally broken. The performance is compared between the vanilla training and masked-modal training. It validates the effect

Table 4. The ablation studies of different components in the proposed CMT.

Im	PC	NDS	mAP	mATE	mASE	mAOE
✓		0.595	0.554	0.515	0.258	0.429
	✓	0.665	0.626	<b>0.372</b>	<b>0.255</b>	<b>0.347</b>
✓	✓	<b>0.669</b>	<b>0.641</b>	0.377	0.254	0.375
(a) Position encoding for query.						
		NDS	mAP	mATE	mASE	mAOE
0.075		0.669	<b>0.641</b>	<b>0.377</b>	0.254	0.375
0.1		<b>0.671</b>	0.638	0.378	<b>0.252</b>	<b>0.334</b>
0.125		0.655	0.624	0.396	0.255	0.397
(c) Voxel size of LiDAR backbone.						
		NDS	mAP	mATE	mASE	mAOE
$800 \times 320$		0.654	0.609	<b>0.374</b>	0.256	0.389
$1600 \times 640$		<b>0.669</b>	<b>0.641</b>	0.377	<b>0.254</b>	<b>0.375</b>
(e) Input size of image backbone.						

PQD	NDS	mAP	mATE	mASE	mAOE
	0.626	0.584	0.429	0.259	0.420
✓	<b>0.669</b>	<b>0.641</b>	<b>0.377</b>	<b>0.254</b>	<b>0.375</b>
(b) Point-based Query Denoise (PQD)					
	NDS	mAP	mATE	mASE	mAOE
ResNet-50	0.658	0.623	<b>0.376</b>	<b>0.253</b>	0.399
ResNet-101	0.664	0.629	0.383	0.254	<b>0.363</b>
VoV-99	<b>0.669</b>	<b>0.641</b>	0.377	0.254	0.375
(d) Image backbone.					
	NDS	mAP	mATE	mASE	mAOE
PointPillars	0.628	0.598	0.430	<b>0.252</b>	0.455
VoxelNet	<b>0.669</b>	<b>0.641</b>	<b>0.377</b>	0.254	<b>0.375</b>
(f) Lidar backbone					

of masked-modal training. Note that the model are only trained with multi-modality and evaluated without any fine-tune process. With vanilla training, the model fails to predict anything meaningful (only Cams with mAP=0) when LiDAR is missing. With masked-modal training, the absence of LiDAR or camera modalities lead to 4.2% and 28.5% NDS drop compared to CMT, respectively. It is observed that losing one modality still remains similar results compared to single-modal training settings. It overcomes the drawback that multi-modal method usually rely on one major modality and performance would degrade significantly if losing the major modality. Especially, for the case of LiDAR missing, the performance is still comparable to the SoTA camera-only method PETR [26], validating the strong robustness of our method.

Moreover, we also investigate the case when any one of cameras fails. Experimental result shows slight performance drop, indicating the tolerable to single camera miss of our method. Six sensors brings an average decrease of 0.7% NDS, no more than 1% performance of the oracle version. The front and back sensor relatively play the important role among camera sensors, with 1.1% and 0.8% decrease respectively, due to their distant or large field of view. Compared to the camera-only setting, our multi-modal framework facilitate the compensation between LiDAR and image domains, thus presenting a robust performance.

#### 4.5. Ablations

We present the ablation studies in Tab. 4. All the experiments are conducted for 20 epochs without CBGS [31].

We first ablate the effect of Im PE and PC PE on the generation of position-guided queries (see Tab. 4 (a)). It shows

that removing PC PE introduces a 7.4%/8.70% NDS/mAP performance drop, which is much larger than the drop of removing Im PE 0.4%/1.5%. Next, we explore the effectiveness of our proposed PQD, as shown in Tab. 4(b). We can easily find that PQD can greatly improve the overall performance by 4.3%/5.7% NDS/mAP. With PQD, the training convergence can be boosted, which is similar to the practice in DN-DETR [19]. Further, Tab. 4 (c-f) illustrates the effect of scaling up the CMT model as well as the input size. Overall, CMT can benefit from the scaling model size. Interestingly, we find increasing the voxel number (smaller voxel size) and image size achieves similar improvements  $\approx 1.5\%$  in NDS. While scaling the image size increases more mAP than the voxel number (+3.2% vs. +1.7%). When increasing the image size from  $800 \times 320$  to  $1600 \times 640$ , we find the performance improvements are mainly from these small objects, such as pedestrian and motorcycle. We also conduct experiments on replacing image and LiDAR backbones, we use VoV-99 [18] and ResNet [13] as our image backbones. Experiments show that our proposed CMT can benefit from larger backbones. For image, VoV-99 backbone achieves the best result and outperforms the ResNet-50 by 1.1%/1.8% in NDS/mAP. While for LiDAR, VoxelNet outperforms the PointPillar by 4.1%/4.3% in NDS/mAP.

#### 4.6. Analysis

CMT is a direct and easy pipeline for multi-modal fusion and can be easily extended. Moreover, benefiting from DETR [3] framework and our training schedule, CMT shows strong robustness under sensor miss conditions. We present some attempted experiments in this section.

**Data extension.** Multi-frame is now a common setting in

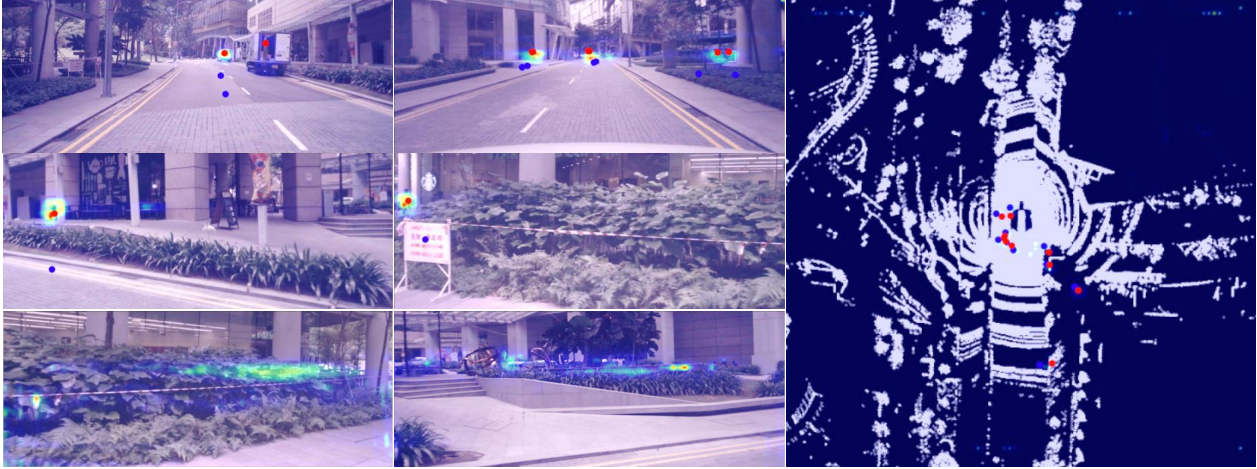


Figure 6. Visualization of attention maps on multi-view images and BEV point clouds. The blue points (●) are the initialized anchor points while red points (●) are the corresponding centers of box predictions. It can be easily found that the high response regions of attention maps mainly focus on the foreground objects, closest to the anchor points.

camera-based 3D object detection [14, 23, 27]. Using multi frames often outperforms the single frame by a clear margin and can solve some typical occlusion problem. We follow the multi-frame alignment in PETRv2 [27]. Considering the high memory cost of multi-frames, we conduct our experiment with a  $800 \times 320$  image resolution. As shown in Tab. 5, adding image frame only improves the NDS/mAP by 0.2%/0.7%. More image frames rarely improve the performance with multi-modal fusion.

Radar has advantages in long range detection and the robustness of extreme weather. Following FUTR3D [8], we stack points from 5 radars together to generate the point cloud. We use several MLP layers to perform coordinates encoding on Radar features, the same as LiDAR. Tab. 5 shows that adding Radar data to our pipeline degrades the performance by 0.9% NDS and 0.6% mAP.

**Visualization.** For better understanding on querying from multi-modal tokens, we visualize the attention map of cross-attention on different modalities (see Fig. 6). We can clearly find that the attention maps have higher response on images and point clouds. It shows that our method can implicitly achieve the cross-modal interaction. We visualize the initial anchor points and the center points of predictions. Most anchor points focus on the closest foreground objects. After the interaction with queries in decoder, anchor points gradually access the accurate center points.

Table 5. Results with more image frames or with Radar points.

+Frame	+ Radar	NDS	mAP
		0.698	0.662
✓		<b>0.700</b>	<b>0.669</b>
	✓	0.689	0.656

## 5. Conclusions

In this paper, we propose a fully end-to-end framework for multi-modal 3D object detection. It implicitly encodes the 3D coordinates into the tokens of images and point clouds. With the coordinates encoding, the simple yet effective DETR pipeline can be adopted for multi-modal fusion and end-to-end learning. With masked-modal training, our multi-modal detector can be learned with strong robustness, even if one of multi-modalities are missed. We hope such a simple pipeline design could provide more insights on the end-to-end 3D object detection.

**Limitation:** Though our CMT brings some advantages compared to those existing approaches, it also reveals some limitations. The computation cost is relatively larger due to the large number of multi-modal tokens and the global attention employed in transformer decoder. To solve this problem, some efforts in two directions maybe taken. The first one is to reduce the redundancy of multi-modal tokens. The foreground tokens can be roughly selected with another individual network [43]. The foreground tokens are then input to our network for high-speed inference. Another possible solution is to replace the global attention with other efficient attentions, like deformable attention [56]. One can also employ a small set of object queries since most queries correspond to the empty objects.

## References

- [1] Xuyang Bai, Zeyu Hu, Xinge Zhu, Qingqiu Huang, Yilun Chen, Hongbo Fu, and Chiew-Lan Tai. Transfusion: Robust lidar-camera fusion for 3d object detection with transformers. In *Proceedings of the IEEE/CVF Conference on Computer Vision and Pattern Recognition*, pages 1090–1099, 2022. 1, 3, 5



- [2] Holger Caesar, Varun Bankiti, Alex H Lang, Sourabh Vora, Venice Erin Liong, Qiang Xu, Anush Krishnan, Yu Pan, Giancarlo Baldan, and Oscar Beijbom. nuscenes: A multi-modal dataset for autonomous driving. In *Proceedings of the IEEE/CVF conference on computer vision and pattern recognition*, pages 11621–11631, 2020. 6
- [3] Nicolas Carion, Francisco Massa, Gabriel Synnaeve, Nicolas Usunier, Alexander Kirillov, and Sergey Zagoruyko. End-to-end object detection with transformers. In *European conference on computer vision*, pages 213–229. Springer, 2020. 1, 3, 7
- [4] Nicolas Carion, Francisco Massa, Gabriel Synnaeve, Nicolas Usunier, Alexander Kirillov, and Sergey Zagoruyko. End-to-end object detection with transformers. In *European conference on computer vision*, pages 213–229. Springer, 2020. 2
- [5] Qiang Chen, Xiaokang Chen, Gang Zeng, and Jingdong Wang. Group detr: Fast training convergence with decoupled one-to-many label assignment. *arXiv preprint arXiv:2207.13085*, 2022. 3
- [6] Qiang Chen, Jian Wang, Chuchu Han, Shangang Zhang, Zexian Li, Xiaokang Chen, Jiahui Chen, Xiaodi Wang, Shumin Han, Gang Zhang, Haocheng Feng, Kun Yao, Junyu Han, Errui Ding, and Jingdong Wang. Group detr v2: Strong object detector with encoder-decoder pretraining. 2022. 3
- [7] Xiaozhi Chen, Huimin Ma, Ji Wan, Bo Li, and Tian Xia. Multi-view 3d object detection network for autonomous driving. In *Proceedings of the IEEE conference on Computer Vision and Pattern Recognition*, pages 1907–1915, 2017. 5
- [8] Xuanyao Chen, Tianyuan Zhang, Yue Wang, Yilun Wang, and Hang Zhao. Futr3d: A unified sensor fusion framework for 3d detection. *arXiv preprint arXiv:2203.10642*, 2022. 1, 3, 5, 8
- [9] Simon Doll, Richard Schulz, Lukas Schneider, Viviane Benzin, Markus Enzweiler, and Hendrik Lensch. Spatialdetr: Robust scalable transformer-based 3d object detection from multi-view camera images with global cross-sensor attention. In *European Conference on Computer Vision*, pages 230–245. Springer, 2022. 2
- [10] Bin Dong, Fangao Zeng, Tiancai Wang, Xiangyu Zhang, and Yichen Wei. Solq: Segmenting objects by learning queries. *Advances in Neural Information Processing Systems*, 34, 2021. 1
- [11] Lue Fan, Xuan Xiong, Feng Wang, Naiyan Wang, and Zhaoxiang Zhang. Rangedetr: In defense of range view for lidar-based 3d object detection. In *Proceedings of the IEEE/CVF International Conference on Computer Vision*, pages 2918–2927, 2021. 2
- [12] Yuxin Fang, Shusheng Yang, Xinggang Wang, Yu Li, Chen Fang, Ying Shan, Bin Feng, and Wenyu Liu. Instances as queries. *Proc. IEEE Conf. Comp. Vis. Patt. Recogn.*, 2021. 1
- [13] Kaiming He, Xiangyu Zhang, Shaoqing Ren, and Jian Sun. Deep residual learning for image recognition. In *Proceedings of the IEEE conference on computer vision and pattern recognition*, pages 770–778, 2016. 6, 7
- [14] Junjie Huang and Guan Huang. Bevdetr4d: Exploit temporal cues in multi-camera 3d object detection. *arXiv preprint arXiv:2203.17054*, 2021. 8
- [15] Junjie Huang, Guan Huang, Zheng Zhu, and Dalong Du. Bevdetr: High-performance multi-camera 3d object detection in bird-eye-view. *arXiv preprint arXiv:2112.11790*, 2021. 2, 5, 6
- [16] Ding Jia, Yuhui Yuan, Haodi He, Xiaopei Wu, Haojun Yu, Weihong Lin, Lei Sun, Chao Zhang, and Han Hu. Detsr with hybrid matching. *arXiv preprint arXiv:2207.13080*, 2022. 3
- [17] Alex H Lang, Sourabh Vora, Holger Caesar, Lubing Zhou, Jiong Yang, and Oscar Beijbom. Pointpillars: Fast encoders for object detection from point clouds. In *Proceedings of the IEEE/CVF conference on computer vision and pattern recognition*, pages 12697–12705, 2019. 2, 4, 6
- [18] Youngwan Lee and Jongyoul Park. Centermask: Real-time anchor-free instance segmentation. In *Proceedings of the IEEE/CVF conference on computer vision and pattern recognition*, pages 13906–13915, 2020. 6, 7
- [19] Feng Li, Hao Zhang, Shilong Liu, Jian Guo, Lionel M Ni, and Lei Zhang. Dn-detr: Accelerate detr training by introducing query denoising. In *Proceedings of the IEEE/CVF Conference on Computer Vision and Pattern Recognition*, pages 13619–13627, 2022. 2, 3, 4, 7
- [20] Yanwei Li, Yilun Chen, Xiaojuan Qi, Zeming Li, Jian Sun, and Jiaya Jia. Unifying voxel-based representation with transformer for 3d object detection. *arXiv preprint arXiv:2206.00630*, 2022. 1, 3, 5
- [21] Yinhao Li, Zheng Ge, Guanyi Yu, Jinrong Yang, Zengran Wang, Yukang Shi, Jianjian Sun, and Zeming Li. Bevdepth: Acquisition of reliable depth for multi-view 3d object detection. *arXiv preprint arXiv:2206.10092*, 2022. 2
- [22] Zhichao Li, Feng Wang, and Naiyan Wang. Lidar r-cnn: An efficient and universal 3d object detector. In *Proceedings of the IEEE/CVF Conference on Computer Vision and Pattern Recognition*, pages 7546–7555, 2021. 2
- [23] Zhiqi Li, Wenhai Wang, Hongyang Li, Enze Xie, Chonghao Sima, Tong Lu, Qiao Yu, and Jifeng Dai. Bevformer: Learning bird’s-eye-view representation from multi-camera images via spatiotemporal transformers. *arXiv preprint arXiv:2203.17270*, 2022. 2, 3, 8
- [24] Tingting Liang, Hongwei Xie, Kaicheng Yu, Zhongyu Xia, Zhiwei Lin, Yongtao Wang, Tao Tang, Bing Wang, and Zhi Tang. Bevfusion: A simple and robust lidar-camera fusion framework. *arXiv preprint arXiv:2205.13790*, 2022. 1, 3, 5
- [25] Shilong Liu, Feng Li, Hao Zhang, Xiao Yang, Xianbiao Qi, Hang Su, Jun Zhu, and Lei Zhang. Dab-detr: Dynamic anchor boxes are better queries for detr. *arXiv preprint arXiv:2201.12329*, 2022. 3
- [26] Yingfei Liu, Tiancai Wang, Xiangyu Zhang, and Jian Sun. Petr: Position embedding transformation for multi-view 3d object detection. *arXiv preprint arXiv:2203.05625*, 2022. 1, 2, 4, 5, 6, 7
- [27] Yingfei Liu, Junjie Yan, Fan Jia, Shuailin Li, Qi Gao, Tiancai Wang, Xiangyu Zhang, and Jian Sun. Petr v2: A unified framework for 3d perception from multi-camera images. *arXiv preprint arXiv:2206.01256*, 2022. 1, 2, 3, 8
- [28] Zhijian Liu, Haotian Tang, Alexander Amini, Xinyu Yang, Huizi Mao, Daniela Rus, and Song Han. Bevfusion: Multi-task multi-sensor fusion with unified bird’s-eye view representation. *arXiv preprint arXiv:2205.13542*, 2022. 1, 3, 5

- [29] Ilya Loshchilov and Frank Hutter. Decoupled weight decay regularization. *arXiv preprint arXiv:1711.05101*, 2017. 6
- [30] Tim Meinhardt, Alexander Kirillov, Laura Leal-Taixe, and Christoph Feichtenhofer. Trackformer: Multi-object tracking with transformers. *arXiv preprint arXiv:2101.02702*, 2021. 1
- [31] Chao Peng, Tete Xiao, Zeming Li, Yuning Jiang, Xiangyu Zhang, Kai Jia, Gang Yu, and Jian Sun. Megdet: A large mini-batch object detector. In *Proceedings of the IEEE conference on Computer Vision and Pattern Recognition*, pages 6181–6189, 2018. 7
- [32] Jonah Philion and Sanja Fidler. Lift, splat, shoot: Encoding images from arbitrary camera rigs by implicitly unprojecting to 3d. In *European Conference on Computer Vision*, pages 194–210. Springer, 2020. 2
- [33] Charles R Qi, Wei Liu, Chenxia Wu, Hao Su, and Leonidas J Guibas. Frustum pointnets for 3d object detection from rgb-d data. In *Proceedings of the IEEE conference on computer vision and pattern recognition*, pages 918–927, 2018. 2
- [34] Charles R Qi, Hao Su, Kaichun Mo, and Leonidas J Guibas. Pointnet: Deep learning on point sets for 3d classification and segmentation. In *Proceedings of the IEEE conference on computer vision and pattern recognition*, pages 652–660, 2017. 2
- [35] Charles Ruizhongtai Qi, Li Yi, Hao Su, and Leonidas J Guibas. Pointnet++: Deep hierarchical feature learning on point sets in a metric space. *Advances in neural information processing systems*, 30, 2017. 2
- [36] Shaoshuai Shi, Xiaogang Wang, and Hongsheng Li. Pointcnn: 3d object proposal generation and detection from point cloud. In *Proceedings of the IEEE/CVF conference on computer vision and pattern recognition*, pages 770–779, 2019. 2
- [37] Leslie N Smith. Cyclical learning rates for training neural networks. In *2017 IEEE winter conference on applications of computer vision (WACV)*, pages 464–472. IEEE, 2017. 6
- [38] Pei Sun, Weiyue Wang, Yuning Chai, Gamaleldin Elsayed, Alex Bewley, Xiao Zhang, Cristian Sminchisescu, and Dragomir Anguelov. Rsn: Range sparse net for efficient, accurate lidar 3d object detection. In *Proceedings of the IEEE/CVF Conference on Computer Vision and Pattern Recognition*, pages 5725–5734, 2021. 2
- [39] Sourabh Vora, Alex H Lang, Bassam Helou, and Oscar Beijbom. Pointpainting: Sequential fusion for 3d object detection. In *Proceedings of the IEEE/CVF conference on computer vision and pattern recognition*, pages 4604–4612, 2020. 5
- [40] Chunwei Wang, Chao Ma, Ming Zhu, and Xiaokang Yang. Pointaugmenting: Cross-modal augmentation for 3d object detection. In *Proceedings of the IEEE/CVF Conference on Computer Vision and Pattern Recognition*, pages 11794–11803, 2021. 5
- [41] Tai Wang, ZHU Xinge, Jiangmiao Pang, and Dahua Lin. Probabilistic and geometric depth: Detecting objects in perspective. In *Conference on Robot Learning*, pages 1475–1485. PMLR, 2022. 2
- [42] Tai Wang, Xinge Zhu, Jiangmiao Pang, and Dahua Lin. Fcos3d: Fully convolutional one-stage monocular 3d object detection. In *Proceedings of the IEEE/CVF International Conference on Computer Vision*, pages 913–922, 2021. 2
- [43] Yulin Wang, Zhaoxi Chen, Haojun Jiang, Shiji Song, Yizeng Han, and Gao Huang. Adaptive focus for efficient video recognition. In *Proceedings of the IEEE/CVF International Conference on Computer Vision*, pages 16249–16258, 2021. 8
- [44] Yue Wang, Alireza Fathi, Abhijit Kundu, David A Ross, Caroline Pantofaru, Tom Funkhouser, and Justin Solomon. Pillar-based object detection for autonomous driving. In *European Conference on Computer Vision*, pages 18–34. Springer, 2020. 2
- [45] Yue Wang, Guizilini Vitor Campagnolo, Tianyuan Zhang, Hang Zhao, and Justin Solomon. Detr3d: 3d object detection from multi-view images via 3d-to-2d queries. In *In Conference on Robot Learning*, pages 180–191, 2022. 1, 2, 5, 6
- [46] Yingming Wang, Xiangyu Zhang, Tong Yang, and Jian Sun. Anchor detr: Query design for transformer-based detector. *arXiv preprint arXiv:2109.07107*, 2021. 4, 5
- [47] Shaoqing Xu, Dingfu Zhou, Jin Fang, Junbo Yin, Zhou Bin, and Liangjun Zhang. Fusionpainting: Multimodal fusion with adaptive attention for 3d object detection. In *2021 IEEE International Intelligent Transportation Systems Conference (ITSC)*, pages 3047–3054. IEEE, 2021. 5
- [48] Yan Yan, Yuxing Mao, and Bo Li. Second: Sparsely embedded convolutional detection. *Sensors*, 18(10):3337, 2018. 4
- [49] Zetong Yang, Yanan Sun, Shu Liu, and Jiaya Jia. 3dssd: Point-based 3d single stage object detector. In *Proceedings of the IEEE/CVF conference on computer vision and pattern recognition*, pages 11040–11048, 2020. 2
- [50] Tianwei Yin, Xingyi Zhou, and Philipp Krahenbuhl. Center-based 3d object detection and tracking. In *Proceedings of the IEEE/CVF conference on computer vision and pattern recognition*, pages 11784–11793, 2021. 2, 5
- [51] Fangao Zeng, Bin Dong, Yuang Zhang, Tiancai Wang, Xiangyu Zhang, and Yichen Wei. Motr: End-to-end multiple-object tracking with transformer. In *European Conference on Computer Vision*, pages 659–675. Springer, 2022. 1
- [52] Gongjie Zhang, Zhipeng Luo, Yingchen Yu, Kaiwen Cui, and Shijian Lu. Accelerating detr convergence via semantic-aligned matching. In *Proceedings of the IEEE/CVF Conference on Computer Vision and Pattern Recognition (CVPR)*, pages 949–958, June 2022. 3
- [53] Hao Zhang, Feng Li, Shilong Liu, Lei Zhang, Hang Su, Jun Zhu, Lionel M Ni, and Heung-Yeung Shum. Dino: Detr with improved denoising anchor boxes for end-to-end object detection. *arXiv preprint arXiv:2203.03605*, 2022. 3, 4
- [54] Yin Zhou and Oncel Tuzel. Voxelnet: End-to-end learning for point cloud based 3d object detection. In *Proceedings of the IEEE conference on computer vision and pattern recognition*, pages 4490–4499, 2018. 2, 3, 4, 6
- [55] Benjin Zhu, Zhengkai Jiang, Xiangxin Zhou, Zeming Li, and Gang Yu. Class-balanced grouping and sampling for point cloud 3d object detection. *arXiv preprint arXiv:1908.09492*, 2019. 6
- [56] Xizhou Zhu, Weijie Su, Lewei Lu, Bin Li, Xiaogang Wang, and Jifeng Dai. Deformable detr: Deformable trans-

formers for end-to-end object detection. *arXiv preprint*  
*arXiv:2010.04159*, 2020. [1](#), [3](#), [8](#)